Journal of the Korean Society of Oceanography
Vol. 38, No. 4, pp. 173 — 184 December 2003

Comparison of the Wind Speed from an Atmospheric Pressure Map (Na Wind) and Satellite Scatterometer-observed Wind Speed (NSCAT) over the East (Japan) Sea

KYUNG-AE PARK*, KYUNG-RYUL KIM, KUH KIM, JONG YUL CHUNG, AND PETER C. CORNILLON[1]
School of Earth and Environmental Sciences, Seoul National University, Seoul 151-742, Korea
Research Institute of Oceanography, Seoul National University, Seoul 151-742, Korea
[1]*Graduate School of Oceanography, University of Rhode Island, RI 02882, USA*

Major differences between wind speeds from atmospheric pressure maps (Na wind) and near-surface wind speeds derived from satellite scatterometer (NSCAT) observations over the East (Japan) Sea have been examined. The root-mean-square errors of Na wind and NSCAT wind speeds collocated with Japanese Meteorological Agency (JMA) buoy winds are about 3.84 ms^{-1} and 1.53 ms^{-1}, respectively. Time series of NSCAT wind speeds showed a high coherency of 0.92 with the real buoy measurements and contained higher spectral energy at low frequencies (>3 days) than the Na wind. The magnitudes of monthly Na winds are lower than NSCAT winds by up to 45%, particularly in September 1996. The spatial structures between the two are mostly coherent on basin-wide large scales; however, significant differences and energy loss are found on a spatial scale of less than 100 km. This was evidenced by the temporal EOFs (Empirical Orthogonal Functions) of the two wind speed data sets and by their two-dimensional spectra. Since the Na wind was based on the atmospheric pressures on the weather map, it overlooked small-scale features of less than 100 km. The center of the cold-air outbreak through Vladivostok, expressed by the Na wind in January 1997, was shifted towards the North Korean coast when compared with that of the NSCAT wind, whereas NSCAT winds revealed its temporal evolution as well as spatial distribution.

Key words: Na wind, satellite scatterometer, NSCAT, wind speed, the East Sea, coherency, EOF, cold-air outbreak, the East Korea Bay

INTRODUCTION

This study was motivated by interest in estimating the CO_2 gas exchange coefficient between the atmosphere and the ocean in the East Sea. The ocean absorbs the anthropogenic carbon in the atmosphere through the carbon dioxide flux between the atmosphere and the ocean, which is governed by the gas exchange coefficient. Wind speed, along with sea surface temperature (SST) and sea state, is a key parameter influencing the coefficient. Thus, derivations of accurate wind field and SST are of importance in the estimation of the CO_2 gas exchange coefficient in order to understand the air-sea fluxes. Recent endeavors to improve this estimation have been made utilizing more accurate satellite-derived SST and scatterometer-observed sea surface winds instead of shipboard measurements with their limitations of spatial and temporal data sampling (Carr *et al.*, 2002).

The longstanding desire to obtain more accurate winds have promoted development and improvement of the satellite scatterometer, which is a microwave radar instrument designed to measure near-surface wind velocity under all weather conditions. The first spaceborne scatterometer was flown on Skylab in 1973, but operated for only a few months, from June to October 1978. The scatterometer on the European Space Agency's Earth Remote Sensing (ERS-1 and 2) mission is a single-swath scatterometer. The NASA Scatterometer (NSCAT) is the first dual-swath Ku-band spaceborne scatterometer. NSCAT was in operation for 10 months from September 1996 to June 1997. Although the NSCAT only lived for a short period, its data record is of great scientific interest and has been extensively used until now. The NSCAT was designed to have an accuracy of wind vectors

*Corresponding author: pka@eddies.snu.ac.kr

less than 2 ms^{-1} in speed and 20 degrees in direction with a spatial resolution of 25 km (JPL, 1998). As a successor of NSCAT, the QuikSCAT/SeaWinds has been operating successfully with superior spatial and temporal coverage since July 1999.

Comparison of satellite-scatterometer winds and other wind products, such as European Centre for Medium Range Weather Forecasts (ECMWF) 10-m winds, has been made for the winds over the global ocean. Liu *et al.* (1998) presented evidence that NSCAT provides global ocean-surface fields with more structure than numerical the weather prediction of ECMWF. Kelly *et al.* (1999) also showed significant differences between NSCAT winds and ECMWF winds in most of the tropical Pacific Ocean. In the seas around Korea, Lee (1998) described the spatial distributions of wind stress, wind stress curl, and wind-driven transport in the East Sea and the Yellow Sea using NSCAT winds and partly mentioned some differences of wind stress curl distribution with the sea surface wind field produced by Na *et al.* (1997). We call this wind field the 'Na wind' hereafter.

The Na wind is the most renowned among the pre-existing wind data sets over the adjacent seas of Korea. It was calculated from atmospheric pressure on twice or four-times daily weather maps by using the Cardone model (Cardone, 1969). Over the past decade, the Na wind has made a great contribution to our understanding of the main characteristics of sea-surface winds, wind stress, and wind stress curl in the seas around Korea (Na *et al.*, 1992; Na *et al.*, 1997). It has been extensively used in numerical model experiments as an input data by many oceanographers in (e.g. Kim and Yoon, 1996). In spite of importance of the Na wind, comparison of wind speeds between NSCAT and the Na wind over the East Sea has not been reported in detail. Therefore, a more quantitative comparison of its differences to other wind fields is strongly desired. It would be very timely to examine what differences exist between the wind fields. Currently, Seawinds instrument on QuikSCAT and ADEOS-II provides wind field with better spatial coverage than NSCAT. However, recent Na wind data (available from 1978 to 1997) are unavailable, so NSCAT wind vectors are used in this study.

Since the Na wind and NSCAT wind products have substantial differences in their origins and generation procedures, marked differences between the two are expected. Considering their differences in spatial and temporal resolution, the two wind fields were re-generated to monthly winds on a 0.25°×0.25° grid to have same intervals in space and time. The main objective of this study is to compare Na wind speed and NSCAT-observed wind speed. We have focused on major differences between the two data products in terms of magnitude of monthly wind speed, its spatial structure and temporal variations.

DATA AND PROCESSING

The Na wind product consists of 6-hourly, 10-m wind vectors on a 0.5°×0.5° grid for the period, January 1978 to December 1997 (Table 1). NSCAT observes wind vectors twice daily on average with a spatial resolution of 25 km (JPL, 1998). In this study, we have used NSCAT level2B swath wind vectors of which time intervals at a given grid are not always same depending on revisiting period of ADEOS satellite.

Fig. 1 shows wind vector cells of each NSCAT swath in which the colored numbers stand for hours. NSCAT covers the entire East Sea in one or two days completely, where some swathes overlap and give multiple observations. In order to compare them, both Na wind and NSCAT wind data are reproduced on the same spatial grid and temporal range. The spatial grid used for the monthly average was determined to 0.25°×0.25°. The height of the Na wind coincides with that of NSCAT winds at 10 m. However, buoy winds, used for accuracy assessment, are measured at 7.5 m. Therefore, the buoy winds were converted to 10-m winds by using LKB model (Liu *et al.*, 1979).

There are two simple ways to derive monthly-averaged wind speeds. One is to calculate a speed mean by taking the average of all wind speeds over a month which have already been calculated from each east-

Table 1. Time and space resolution of Na Wind and NSCAT wind. Time interval of NSCAT wind at a given point depends on revisiting period of ADEOS satellite

	Na Wind	NSCAT
Time resolution	6 hours	2~24 hours
Space resolution	0.5°×0.5°	25 km × 25 km
Time span	Jan. 1978 ~ Dec. 1997	Sep. 1996 ~ Jun. 1997
Height from sea surface	10 m	10 m

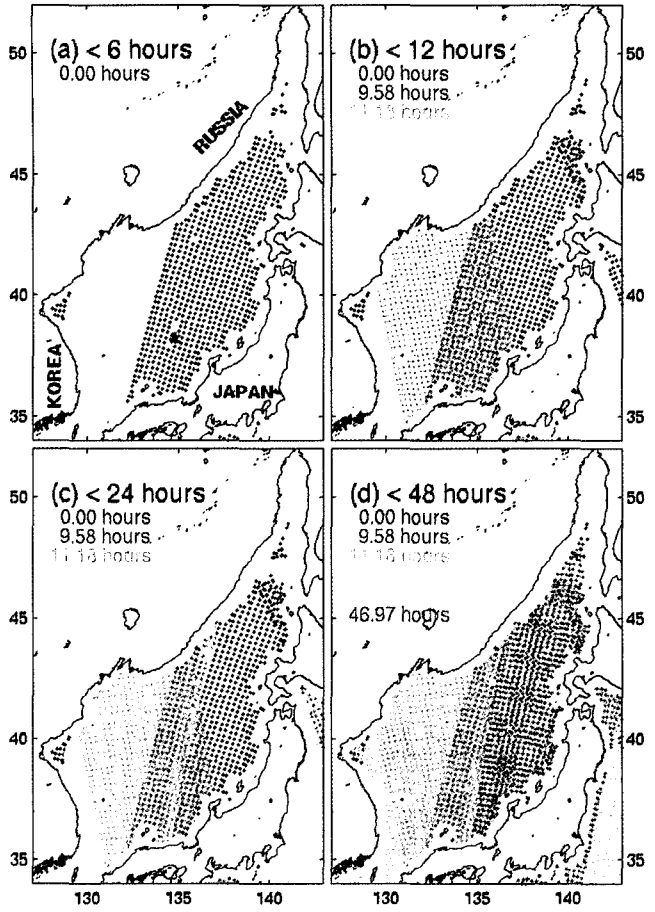

Fig. 1. Spatial and temporal coverage of NSCAT wind vector cells within (a) 6 hours, (b) 12 hours, (c) 24 hours, and (d) 48 hours. Location of JMA buoy (#21002) is marked as a red asterisk at 134°33'E, 37°55'N.

ward (U) and northward component (V) of a wind vector, as shown in Eqn. (1). The other is to use a vector mean to estimate a wind speed mean from wind vectors of which the eastward and northward components are first separately averaged over a month, as shown in Eqn. (2):

$$W_1(i,\ j) = \frac{1}{N}\sum_{t=1}^{N}\sqrt{U(i,j,t)^2 + V(i,j,t)^2} \qquad (1)$$

$$W_2(i,\ j) = \sqrt{\left(\frac{\sum U(i,j,t)}{N}\right)^2 + \left(\frac{\sum V(i,j,t)}{N}\right)^2} \qquad (2)$$

where N is the number of wind vectors. Fig. 2 shows wind speed distributions derived from a NSCAT swath wind vectors over the East Sea in January 1997 based on the Eqns. (1) and (2). While spatial patterns of the two wind speed maps are quite similar, yet their magnitudes show considerable differences: the latter is estimated much lower than the former. The

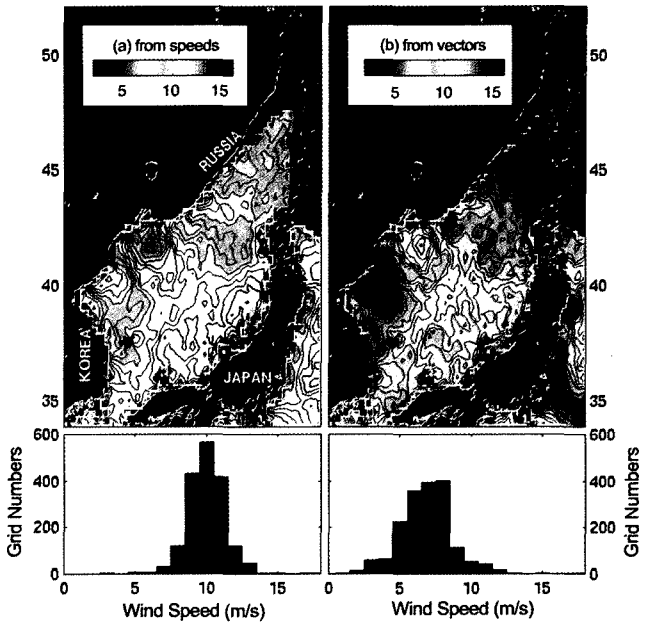

Fig. 2. Differences of mean wind speeds from (a) speed mean and (b) vector mean and their histograms.

lower diagrams of Fig. 2 are histograms of all wind speeds in the upper diagrams. The histogram on the left shows a Gaussian-like distribution of which the maximum peak is found around 10 ms^{-1}, whereas that on the right side is skewed to lower speeds around 8 ms^{-1}. Gas transfer between atmosphere and ocean is not dependent on which direction the wind blows, but on how strong the wind blows over the sea surface. In light of this, the former calculation of mean wind speeds is thought to be more relevant to our objectives, so we have used wind speeds in Fig. 2a based on Eqn. (1).

While constructing monthly wind speed maps, NSCAT wind vectors with poor quality flag and rain flag were all eliminated. Wind vectors with anomalous direction, quite distinct from the overall wind direction of adjacent wind vectors, may come from wind vector ambiguity problems and should be carefully handled in studies in which direction a is very important parameter. Since this study takes into account the wind magnitude only for gas flux estimation, the wind vector ambiguity has not been examined.

RESULTS

Comparison with Buoy Wind

As mentioned earlier, the Na wind and NSCAT wind speed have been estimated from different data

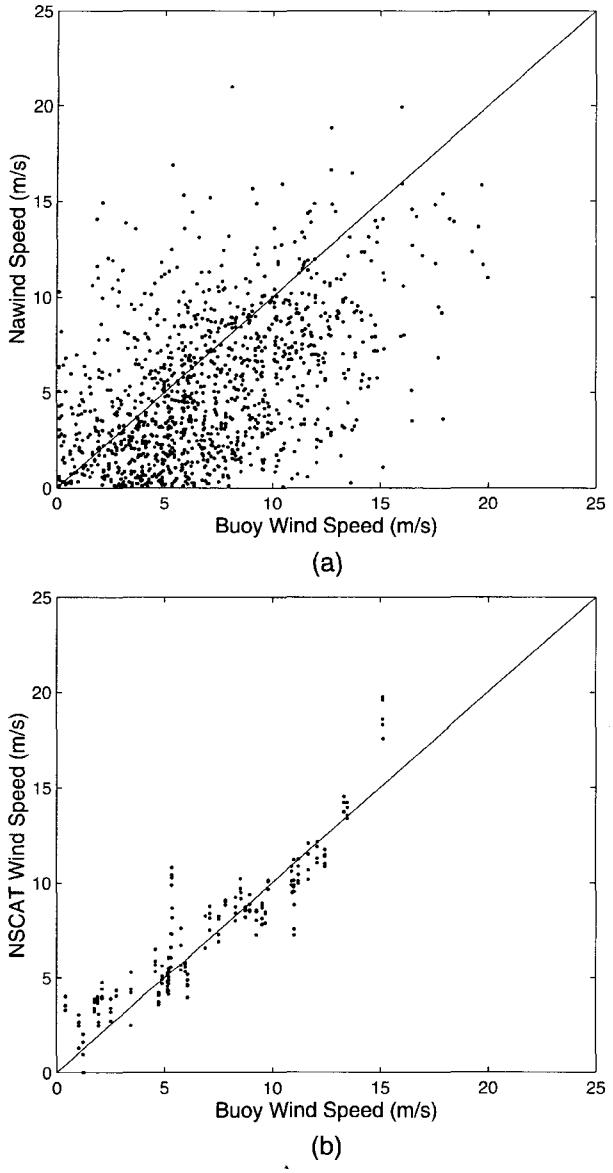

Fig. 3. Scatter plot of (a) Na wind and (b) NSCAT wind speeds collocated with the JMA buoy wind speeds within 30 min.

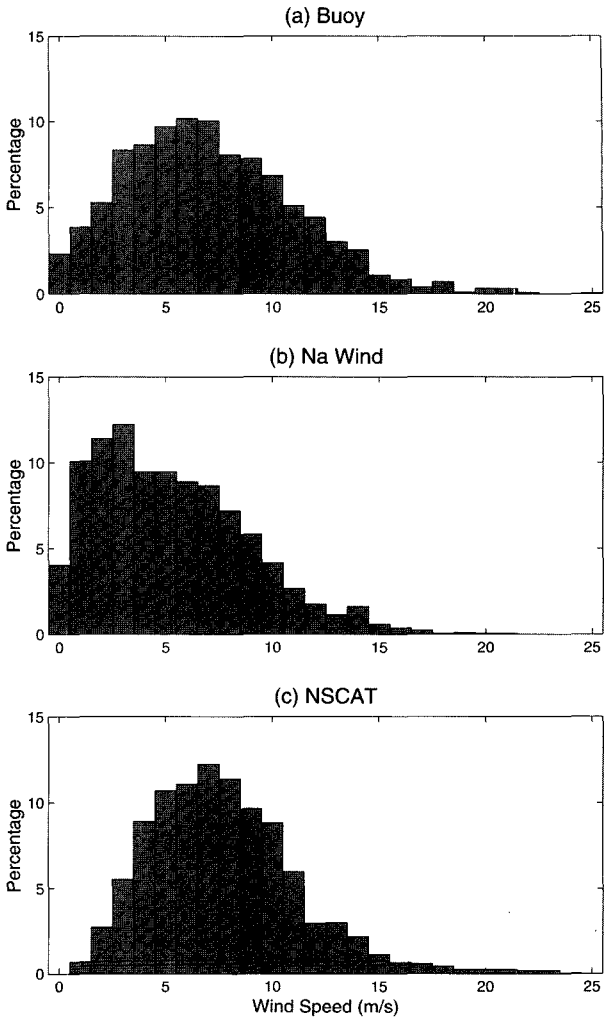

Fig. 4. Histogram (%) of all the wind speeds from (a) JMA buoy, (b) Na wind, and (c) NSCAT collocated at the JMA buoy location for the NSCAT period.

sources and procedures. So it is desirable to examine how their wind speeds coincide with real measurements. Accuracies and spectral characteristics of wind speeds from NSCAT and the Na wind are examined by comparison with winds measured by the JMA buoy (37°55′N, 134°32′E) in the East Sea.

Collocated data set with buoy wind measurements consists of all NSCAT measurements and Na winds acquired within 25 km and 30 min during the NSCAT period. In the matchup procedure, NSCAT wind vectors with poor quality or rain flag were all eliminated. The number of collocated points between Na wind and buoy winds is 1144 and that of NSCAT is quite a small at 182 due to its revisiting period.

Fig. 3 is a scatter plot of Na wind and NSCAT wind speeds to their collocated buoy wind speeds. Small scatters around the linear fit show that there is good correspondence between NSCAT wind and the buoy wind. Its rms error is vary small at 1.53 ms^{-1}. By contrast, the rms difference of Na wind with respect to buoy winds is quite large at 3.84 ms^{-1}. The correlation coefficient between Na wind and the buoy wind is small at 0.49, while that of NSCAT winds and its collocated buoy winds is quite large at 0.91. Thus, this comparison reveals that the Na wind has less accuracy with respect to short-term buoy wind measurements within a short period of 30 minutes. However, there is strong limitation that NSCAT wind has quite a small matchup points due to orbit period and spatial coverage of NSCAT as shown in Fig. 1.

In order to produce time series data, Na wind and NSCAT wind are collocated within a space gap of 0.5° and 25 km, respectively, from the buoy location. As time intervals of the buoy data and Na wind are constant as every 3 hours and 6 hours, respectively, time series of NSCAT winds are linearly interpolated to 12-hourly wind field. Fig. 4 shows histogram of each wind field at the buoy location in which the unit is percentage by dividing number density with total number of wind data. Buoy wind data reveal Gaussian-like distribution centered at 6 ms^{-1}, which is quite similar to NSCAT wind distribution centered at 7 ms^{-1}. By contrast, Na wind speed distributes at a low wind range from 1 ms^{-1} to 3 ms^{-1} with a considerable fraction.

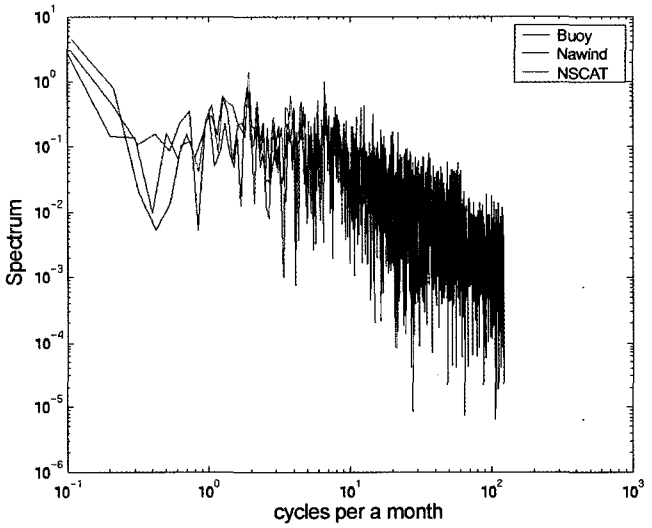

Fig. 5. Spectra of time series of wind speeds from JMA buoy (black), Na wind (blue), and NSCAT (red).

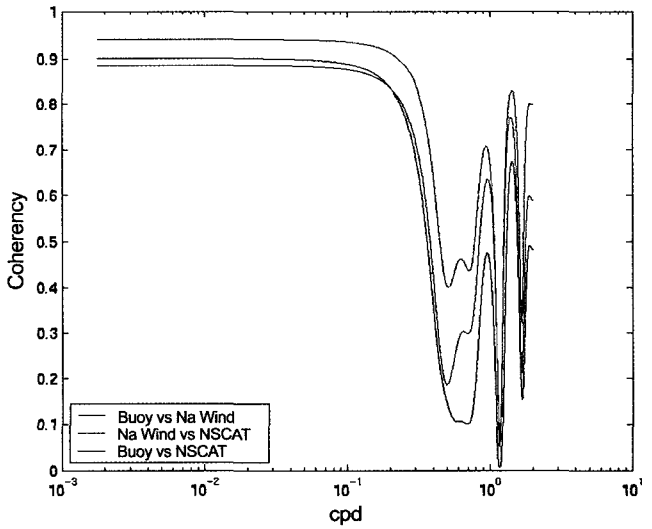

Fig. 6. Coherency of wind speeds from JMA buoy(black), Na wind(blue), and NSCAT(red) as a function of frequency (cycles per a day).

Temporal variations in the true wind field can lead to large differences in the observed wind field depending on data sampling interval. From this point of view, NSCAT wind can lead to increased sampling errors than Na wind or buoy wind. However, even the ocean buoy winds, measured hourly, may also express a different wind field to the true wind of which the temporal variability is extremely large within an hour. Thus, we have compared spectral characteristics of the three winds in Fig. 5. For high frequency greater than 10 cycles per a month (~3 days), spectral density of NSCAT greatly decreases as its temporal sampling capability is poor by 2~24 hours. As this high frequency band, Na wind shows higher spectral energy than ocean buoy winds. For synoptic scales from 3 to 30 days (1~10 cycles per a month), however, NSCAT shows higher peaks of spectral energy than those of Na wind and the buoy wind. For most of

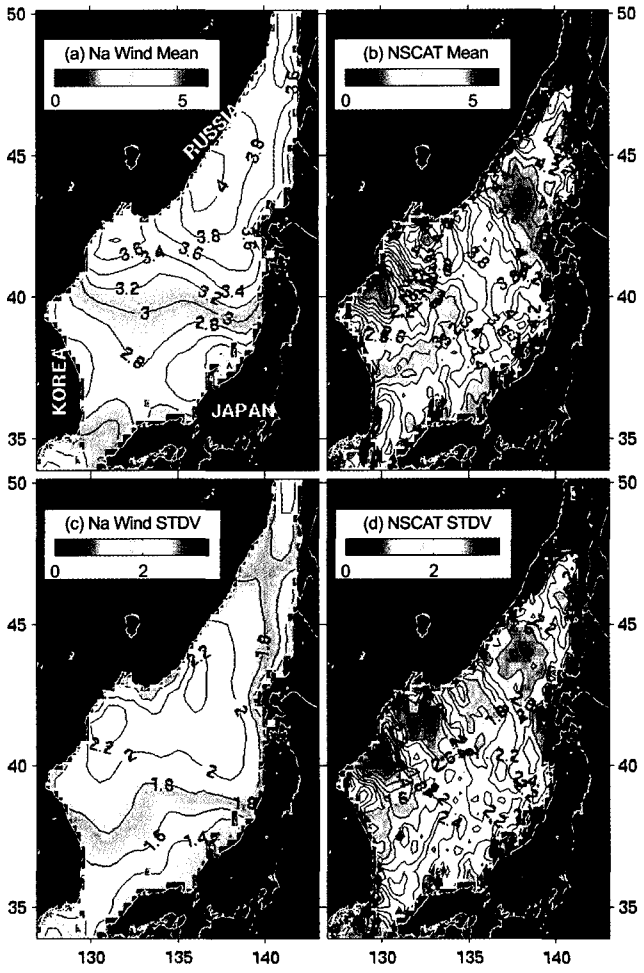

Fig. 7. Mean and standard deviations of wind speeds (ms^{-1}) from (a) Na wind and (b) NSCAT over NSCAT period (September 1996 - June 1997).

long periods except for a spectral drop at frequencies around 4×10^{-1} cycles per a month, NSCAT winds reveal large spectral energy.

Fig. 6 shows coherency between the three wind fields. Each curve shows large coherency greater than 0.88 at small frequencies less than 2×10^{-1} cycles per a day, i.e., long period greater than 5 days. NSCAT wind shows largest coherency with the buoy wind than Na wind does. Coherency curves abruptly decrease from 2×10^{-1} cpd (~5days) and reach minimum at 5×10^{-1} cpd (~2 days).

On the base of the distribution of the wind speed spectra and coincidence with real wind measurements at atmospheric synoptic scale, we chose a temporal range for comparison as one month. Both 6-hourly Na wind and NSCAT swath wind vectors are re-generated to monthly wind fields and compared each other in the following sections to understand what differences exist between the two wind fields.

Differences in temporal mean and variability

Fig. 7 shows the temporal mean of wind speeds from the Na wind and NSCAT over the NSCAT period and their temporal standard deviations. As shown in Fig. 3a, the Na wind shows a typical pattern of wind speeds in which winds are stronger in the northern part of the East Sea than in the southern part. Strong wind speeds of 4 ms^{-1} are found on the Russian coast around 44°N, 137°E, and of 3.6 ms^{-1} south of Vladivostok. The lowest wind speeds, of less than 2.6 ms^{-1}, are observed on the eastern coast of Korea and the western coast of Japan around 37°N. In the case of NSCAT in Fig. 7b, local maxima of mean wind speeds are also found at similar positions to those of Na wind speeds: south of Vladivostok and off the Russian coast. However, apparent differences are detectable along the western coast of Japan south of the Tsugaru Strait where the Na wind speeds are small, less than 2.8 ms^{-1}, but the NSCAT wind speeds are greater than 3.6 ms^{-1}. The other difference between the two is observable from the lowest speeds which are clearly seen from the NSCAT winds, of 2 ms^{-1} east of North Korean coast around 41°N, but which are invisible from the Na wind.

Temporal standard deviations of Na wind show a large variability, greater than 2.2 ms^{-1}, off the North Korean and Russian coasts (Fig. 7c). By contrast, large NSCAT wind variabilities are dominated by winds of more than 2.6 ms^{-1}, not in the area off North Korea but along the downwind direction of a cold-air outbreak from northwest to southeast through Vladivostok. Local maxima off the Russian coast are located farther north than those from the Na Wind. These high variabilities appear interchangeably with low variabilities of less than 1.6 ms^{-1} along the southwestward continental shelf from the Russian coast to the North Korean coast. These plots demonstrate that the NSCAT winds show much more detailed spatial structure than Na wind speeds in terms of magnitude and temporal variability. Another difference is found along Japanese coast where the Na wind shows a calm region with a low temporal variability of 1.4 ms^{-1} whereas the NSCAT wind reveals large values of 2.2 ms^{-1}. One possible explanation for these differences is depicted in the last section.

Differences in monthly maps

Fig. 8 and Fig. 9 show distribution of monthly-averaged wind speeds from the Na wind and NSCAT. Apparently, they are quite similar each other. For example, both winds in September 1996 show local minima of less than 0.5 ms^{-1} in the western part of the East Sea. Other monthly maps also show a coinciding pattern on basin-wide large scales, although the centers of the local minima and maxima are slightly shifted.

However, significant differences between the two are also clearly distinct. One of the largest differences is found in January 1997 when the Siberian cold-air outbreak through Vladivostok is at its strongest. As shown in Fig. 8, the Na wind speed expresses this well-known cold-air outbreak comparably, but its center is shifted considerably westward, toward the North Korean coast, and its magnitude occupies only 70% of the corresponding NSCAT wind speed. Very recently, this cold-air outbreak has been of special interest in understanding cold bottom water formation in the East Sea, circulation in the Japan Basin, and subpolar fronts in the East Sea (e.g. Kawamura and Wu, 1999; Chen *et al.*, 2001; Chu *et al.*, 2001; Dorman et al., 2003). Those researches have a strong requirement for a detailed description of spatial distribution and temporal variation of the cold-air outbreak. Another profound difference is found along the Japanese coast south of 40°N where the Na wind has the lowest, of less than 5.5 ms^{-1}, while the NSCAT wind has large speeds of 8 ms^{-1} in phase with the outbreak. NSCAT winds make it possible to investigate the temporal evolution of the cold northwesterly winds: it begins in October very weakly, becomes

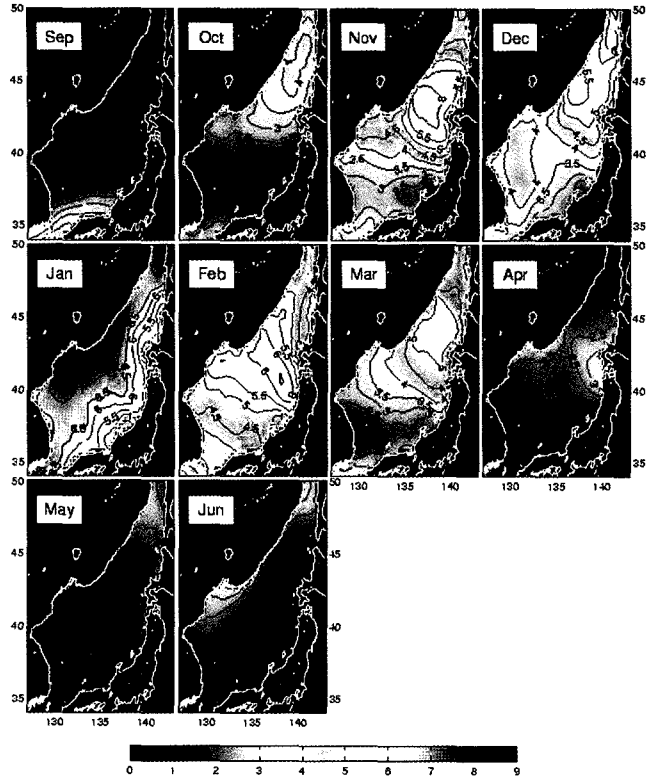

Fig. 8. Monthly mean of wind speeds (ms^{-1}) from Na wind during NSCAT period (September 1996 - June 1997).

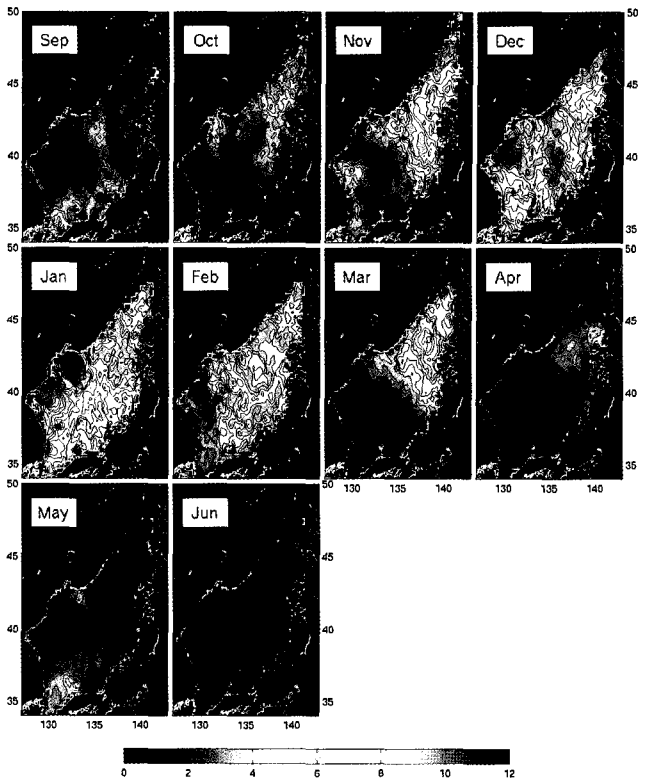

Fig. 9. Monthly mean of wind speeds (ms^{-1}) from NSCAT during NSCAT period (September 1996 - June 1997).

stronger at 6 ms^{-1} in December, achieves its strongest of 12 ms^{-1} in January, and lasts, finishing at 8 ms^{-1}, till February 1997. On the other hand, the Na wind expresses the strongest cold-air outbreak in January 1997 and remains only vaguely in February.

It should be noted that NSCAT observes spatially-dominated strong winds over the East Korea Bay off Wonsan from November 1996 to February 1997. In November, its speed is about 6 ms^{-1} in an area with a presence of a quasi-permanent warm eddy. This feature appears not only in December but also in January, however, the monthly Na wind does not express such a small-scale wind since it is substantially based on a large-scale atmospheric pressure map. These kinds of difference in wind patterns off Wonsan are of importance in understanding the seasonal change of circulation in the region of North Korea, which has been poorly understood until now.

Fig. 10a shows a time series of the spatial mean of monthly-averaged wind speeds from the Na wind and NSCAT over the entire East Sea. Overall, both winds reveal their seasonal variations which are strongest in January and lowest in June during the NSCAT period. One of the major differences is that the Na wind is lower than NSCAT wind from September 1996 through February 1997, particularly by 45% in September 1996, when compared with the NSCAT wind (Fig. 10b). To clarify this, the histograms of all swath NSCAT winds and Na wind speeds, before being registered on the same monthly grids, are plotted in Fig. 12. It also demonstrates that Na wind speeds are distributed at lower range of wind speeds than NSCAT winds except for June in 1997. This feature has been also detected from the comparison with the buoy winds as shown in Fig. 4.

Differences in dominant EOF modes

Both the NSCAT and Na wind fields have shown similar monthly distribution on basin-wide large scales as mentioned earlier. For more quantitative comparisons, temporal empirical orthogonal function analysis is performed on the monthly wind speeds to derive their dominant. Fig. 12 shows the first two EOF modes of Na wind speed and their time-varying coefficients. The first mode accounts for 87.36% of wind speed variance. Its pattern is similar to the temporal variability of Na wind in Fig. 7c. The eigenvectors in Fig. 12a are all negative over the entire study area, with the largest amplitudes of the neg-

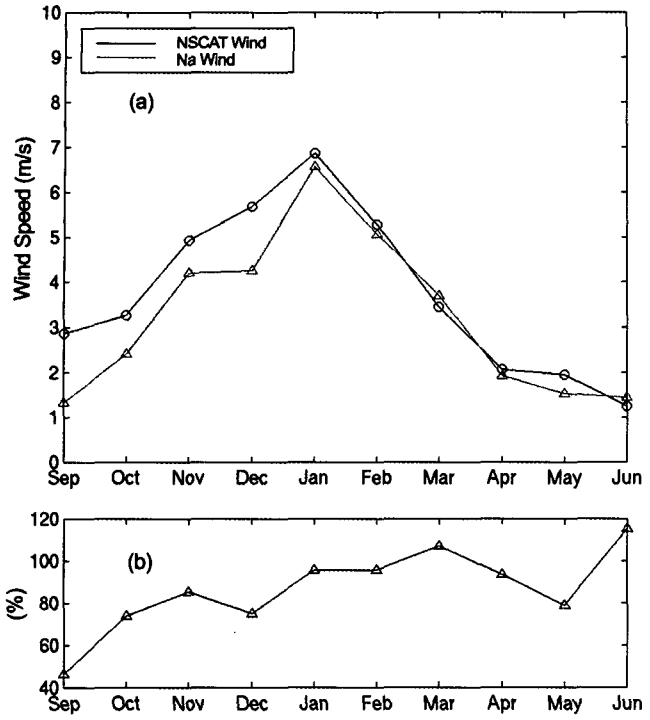

Fig. 10. Monthly variations of (a) spatial mean of wind speeds (NSCAT: black, Na wind: red) and (b) percentage of Na wind speed to NSCAT wind speed during the NSCAT period.

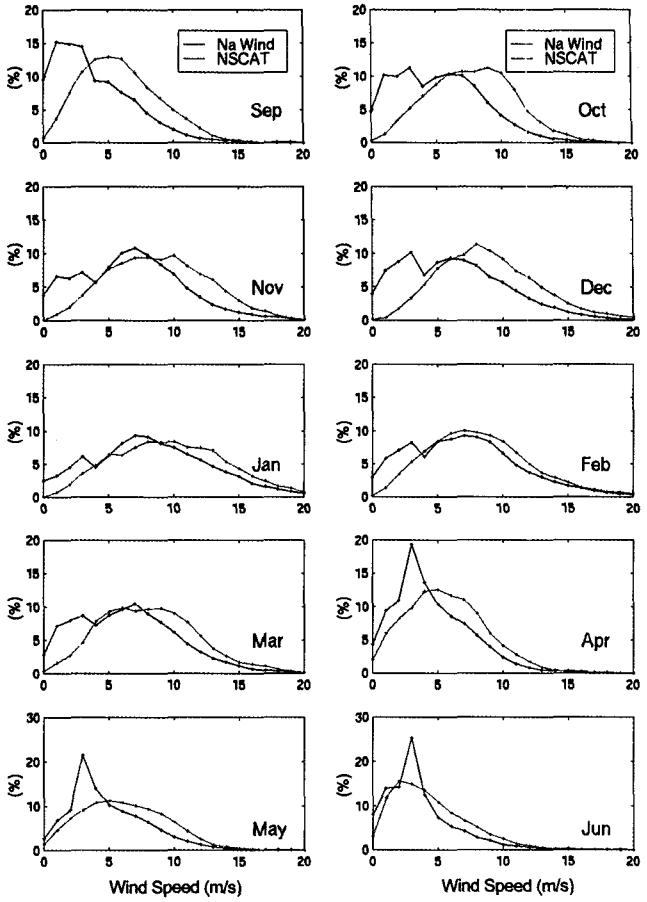

Fig. 11. Monthly histograms of all the Na wind speeds (black) and NSCAT swath wind speeds (red) before monthly mapping.

atives less than −0.03 over regions off the North Korean coast and the northeastern part of the Japan Basin. Its coefficients in Fig. 12b show annual-like variation. The eigenvector multiplied by its corresponding coefficient represents a wind speed deviation from a temporal mean of the original wind speeds. The multiplication is positive from November 1996 through March 1997, and particularly strongest in January, which coincides with the period of the cold-air outbreak.

The second EOF mode of Na wind explains 5.76% of the wind variability. It expresses the main temporal variability of the residual variance after the first mode. The positive maximum appears in the western area off Hokkaido Island and extends to the Russian coast in a large latitudinal range from 40°N to 48°N. The coefficients in Fig. 12d show two positive peaks in excess of 20 in November 1996 and March 1997. It is a very small −28 in September 1996 and also in January 1997, which implies that this region has its weakest winds in January, by contrast with the largest wind speeds of the outbreak in the outsea of Vladivostok, as shown in the first mode. These positive eigenvectors are anti-correlated with most of the southern and western parts of the East Sea. The large coefficients exceeding 20 are found in November and March. These strong winds between the Hokkaido and Russian coasts have not been paid much attention so far, but seem to play a significant role in the circulation of the northern part of the East Sea after the strong Siberian cold-air outbreak disappears and also before it appears.

Fig. 13 shows the first two EOF modes of NSCAT wind speeds and their coefficients as a function of time. The first mode accounts for 66.4% of the total variance which is very small when compared with that of the Na wind (87.36%). Multiplication of the eigenvector with its corresponding coefficient shows a band-like structure in which positive and negative values appear interchangeably along the continental coast from North Korea to Russia. The amplitude of coefficient is strongest at 125 in January during the cold-air outbreak from the Siberian continent. Apparently, this pattern seems to be similar to the first EOF mode of the Na wind, but it has fundamental differences. The center of the lowest eigenvectors of the Na wind is shifted to the west, toward the North

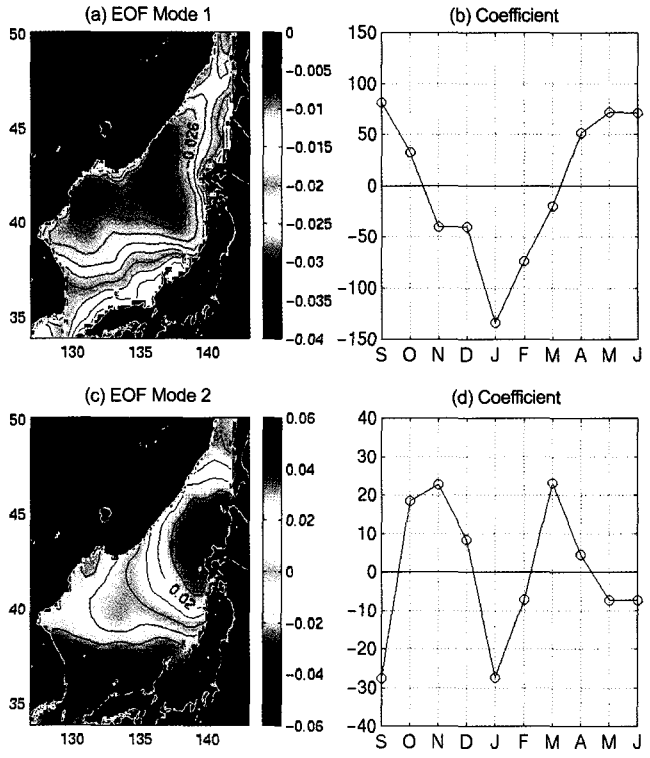

Fig. 12. The first two EOF modes of Na wind speeds and their coefficients.

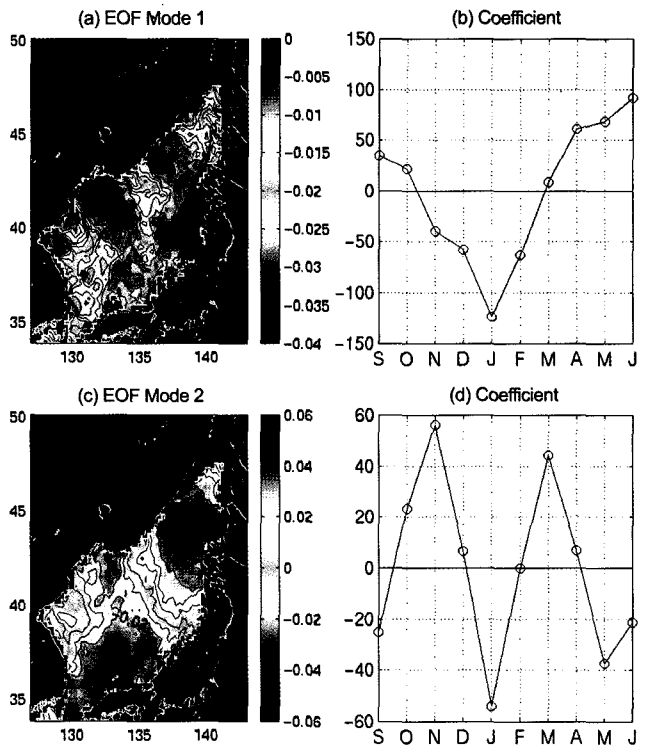

Fig. 13. The first two EOF modes of NSCAT wind speeds and their coefficients.

Korean coast, relative to that of the NSCAT wind. The small negative eigenvectors of the first EOF (> −0.015), in reality weak winds, over regions centered at 40°N, 130°E off North Korean coast and area east of Vladivostok are not detectable from the first mode of the Na wind data (Fig. 12a).

The second mode of NSCAT wind speeds explains 17.27% of the total variance (Fig. 13c). It shows positive eigenvectors over the northeastern part of the East Sea between the Russian coast and Hokkaido. This pattern is quite similar to the second mode of the Na wind as shown in Fig. 12c, but its center is shifted west toward the Russian coast relative to the center of the Na wind. It appears most strongly, not in January, but in November. It coincides with the onset of the predominant cold-air outbreak through Vladivostok. Its temporal coefficients show peaks in November 1996 and March 1997, which is similar

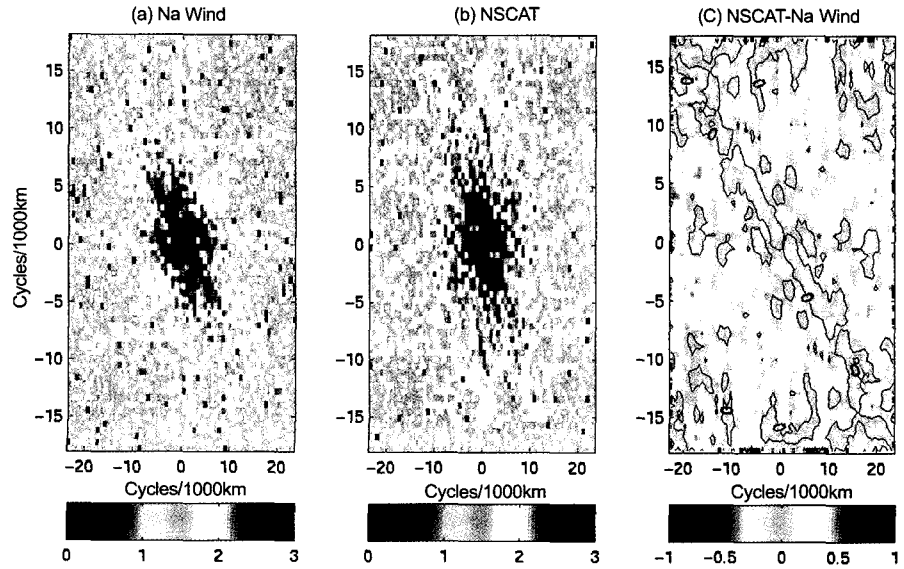

Fig. 14. Two-dimensional spectra of wind speeds from (a) Na wind and (b) NSCAT in January 1997, and (c) their spectral differences (NSCAT - Na wind).

to those of the Na wind. However, there are still large differences between the two monthly winds over the localized area east of the East Korea Bay. Positive cell of 0.02 appears from NSCAT winds, but is not apparent from Na winds.

In fact, there are a few cases that each NSCAT swath failed to cover this region completely within 24 hours. However, we have already shown that NSCAT winds are much closer to the real oceanic buoy winds and contain larger energy than the Na wind at atmospheric synoptic scales of 3~30 days (Figs. 5 and 6). This implies that the monthly wind maps of NSCAT can appropriately represent the meso-scale winds intensified over the narrow region east of the East Korea Bay. By contrast, Na wind may produce this wind over the East Korea Bay in the individual 6-hourly map but seems to lose large energy not enough to remain in the monthly maps.

Differences in wavenumber spectra

Shown in Fig. 14 are two-dimensional spectra of wind speeds from the Na wind and NSCAT in January 1997 and their spectral differences. The energy density of the Na wind (Fig. 14a) tends to be strongly localized at a narrow range of small wavenumbers less than 3 cycles/1000 km, i.e. at large spatial scales, whereas that of the NSCAT wind scatters to larger wavenumbers by 10 cycles/1000 km with considerable energy. Subtraction of the spectrum power of NSCAT winds from that of Na wind shows positive values over most of the high wavenumbers, except for low wavenumbers around zero and along the linear trend of the Na wind spectra from upper left to lower right, as illustrated in Fig. 14c. This means that significant energy loss of small-scale signals occurs in the energy spectrum of the Na wind field. Consequently, it is evident that scatterometer winds retain much more power than Na winds at short wavelengths of less than 200 km (5 cycles/1000 km) approximately. As pointed out earlier, this may come from coarse spatial grid of the Na wind and differences in the retrieval procedure of wind speeds: the Na wind is estimated from a smoothened atmospheric pressure map without real oceanic measurements, while NSCAT observes realistic radar backscattering for each wind vector cell every 25 km.

As mentioned earlier, there are multiple observations in some part of the ocean within a day and no data at all in other part depending on the swath width and revisiting period of NSCAT. These irregularly sampled observations can lead to mapping errors as discontinuity of wind vectors and aliasing of shorter-time scale winds. It has long been studied to minimize these kinds of errors by developing objective mapping of scatterometer wind (e.g. Kelly and Caruso, 1990; Kelly *et al.*, 1999). The latter reported that zonal spectra of daily NSCAT maps had a small spectral peak at 600 km, corresponding to the scatterometer swath width, in the tropical Pacific Ocean. However, it is not possible to find the spectral peak from the present monthly maps for which the length scale of 600 km is around the Nyquist frequency in the East Sea.

Schlax *et al.* (2001) recommended the time resolution for high spatial resolution wind maps as 2~3 weeks for NSCAT and about one week for SeaWinds or QuikSCAT. Most of the mapping algorithms basically act as low-pass filters so that larger space scales and timescales are preferentially retained in the estimates (Schlax *et al.*, 2001). Since this study is analyzing the monthly-averaged maps instead of the daily wind maps as above, we can avoid or minimize that kind of errors. In light of this, it is unlikely that the large NSCAT wind speeds east of the East Korea Bay, shown in the 2nd EOF mode, originate from fallacious winds due to the spatial and temporal limitation of the scatterometer data.

SUMMARY AND CONCLUSION

Satellite scatterometers have provided a quantity of wind vectors over the global ocean, exhibiting high capability of spatial and temporal sampling. This study was motivated by our endeavors to estimate the CO_2 gas exchange coefficient over the East Sea. As a first step, we have compared the scatterometer-derived wind speed with the Na wind and quantitatively described differences in their monthly maps.

Major differences between NSCAT and Na winds result from the differences in data origin, as expected. A NSCAT wind is close to a realistic wind since it was retrieved from real-time observation of radar backscattering at the sea surface, while Na wind is a non-observed wind calculated from the atmospheric pressure distribution in large-scale weather maps with little observation over the sea.

Accuracies of Na wind and NSCAT wind are assessed by comparing them with collocated JMA buoy data within 25 km and 30 min. The Na wind shows large scatters with an rms error of 3.84 ms^{-1} while NSCAT wind shows a small rms error of 1.53 ms^{-1}. Na wind

skewed to a lower wind range than both NSCAT and the buoy winds. For a period of 3~30 days, NSCAT wind data contain higher spectral energy than the Na wind. At this atmospheric synoptic frequency range, NSCAT wind shows highest coherency of 0.94 with the buoy winds than that of the Na wind of 0.88.

On a basin-wide spatial scale, the Na wind shows fairly good agreement with NSCAT wind, as evidenced by their dominant EOFs. However, two-dimensional wavenumber spectra of the wind speeds show that NSCAT winds show much smaller features than Na winds. Due to the difference in spatial scale of data origin and lack of spectral energy at low frequency band, the monthly Na wind did not regenerate the intensified small-scale winds of less than 100 km east of the East Korea Bay off the Wonsan, while NSCAT observed these winds clearly in the monthly map, particularly in November, and shows their changes with time. Both monthly-averaged maps and the second EOF mode of NSCAT winds support the existence of the winds in the outsea of Wonsan. This wind field is unlikely to be spurious winds from monthly mapping errors of irregularly sampled observations as depicted by Schlax *et al.* (2001). These winds may play a significant role in simulating local oceanic circulation properly, which has been poorly understood partly due to lack of shipboard measurements in the North Korean area.

During the Siberian cold-air outbreak through Vladivostok in January 1997, both wind speeds are characterized by large magnitude of winds in the seas south of Vladivostok. However, its center according to the Na wind is considerably shifted to the west toward the North Korean coast when compared with that observed by NSCAT. The Na wind shows it only in January, while NSCAT reveals its temporal evolution from October 1996 through February 1997. There are also striking differences between the two wind fields along the Japanese coast during the cold-air outbreak period. NSCAT winds are strong not only along the downwind side in the seas off Vladivostok, but also along the western coast of Honshu, whereas the corresponding Na wind is very weak. According to our analysis (not shown here), other scatterometer-observed winds such as QuikSCAT and SSM/I also show a high level of coincidence with NSCAT wind. In what does this manifest difference between the Na wind and NSCAT wind lie ? This has never been mentioned as yet as far as we know. One of the possible causes of this difference, we believe, might be that it originates from atmospheric stability in a marine boundary layer (MBL) which cannot be substantially considered in Na wind at all. Scatterometer observations look at real-time backscattering at the sea surface which is affected by sea surface winds, stability in the air, and the sea surface condition as well. Cornillon and Park (2001) and Park and Cornillon (2002) have first mentioned the modification of scatterometer winds due to surface current and atmospheric stability. Detailed explanations of this in the East Sea are in preparation for reporting in another paper.

High capability of spatial and temporal sampling of winds by satellite scatterometers, in spite of their sampling errors, is expected to facilitate better understanding of realistic gas exchange flux between air and sea. In light of this, scatterometer-observed winds are believed to be more appropriate for our current concerns and contribute to better estimation of gas transfer velocity at the air-sea interface in the East Sea. In addition, it is thought that all the differences presented in this study are of significant importance to understanding the oceanic response to different kinds of wind forcings in numerical model experiments (e.g. Horgan and Hurlburt, 2000) and its results should be carefully interpreted.

ACKNOWLEDGEMENTS

This study was performed with support from Ecotechnopia, Ministry of Environment, Korea and the Brain Korea 21 Project through the School of Earth and Environmental Science, SNU. This study was also performed in part with support from U.S. National Aeronautics and Space Administration (Grant NAS5-32965) via Oregon State University as part of the SeaWinds program. NSCAT wind vectors are obtained from PODAAC at the NASA/JPL using DODS (Distributed Oceanographic Data System). We are grateful to Profs. J. Y. Na and Y. J. Ro for their helpful suggestions and comments.

REFERENCES

Cardone, V.J., 1969. Specification of the wind distribution in the marine boundary layer for wave forcasting. New York Univ., School of Engineering and Science, Report GSL-TR69-1, 181pp.

Carr, M.E., W. Tang, W.T. Liu, 2002. CO_2 exchange coefficients from remotely sensed wind speed measurements: SSM/I versus QuikSCAT in 2000, *Geophys. Res. Lett.*, **29**: 1740-1743.

Schlax, M.G., B.C. Chelton, and M.H. Freilich, 2001, Sampling errors in wind fields constructed from single and tandem scatterometer datasets, *J. Atmos. Ocean. Tech.*, **18**: 1014-1036.

Chen, S.S., W. Zhao, J.E. Tenerelli, R. H. Evans, and V. Halliwell, 2001. Impact of the AVHRR sea surface temperature on

atmospheric forcing in the Japan/East Sea. *Geophys. Res. Lett.*, **28**: 4539-4542.

Chu, P.C., J. Lan, and C. FAN, 2001. Japan Sea Thermohaline Structure and Circulation. Part I: Climatology. *J. Phys. Oceanogr.*, **31**: 244-271.

Cornillon, P., and K.-A. Park, 2001. Warm core ring velocities inferred from NSCAT. *Geophys. Res. Lett.*, **28**: 575-578.

Dorman, C.E. R.C. Beardsley, N.A. Dashko, C.A. Friehe, D. Kheilf, K. Cho, R. Limeburner, and S.M. Varlamov, 2003. Winter marine conditions over the Japan Sea, submitted to *J. Geophys. Res.*

Hogan, P.J. and H.E. Hurlburt, 2000, Impact of upper ocean-topographical coupling and isopycnal outcropping in Japan/East Sea models with 1/8° to 1/64° resolution, *J. Phys. Oceanogr.*, **30**: 2535-2561.

Jet Propulsion Laboratory, 1998. Science Data Product (NSCAT-2) User's Manual Ver. 1.2, Overview and Geophysical Data Products. *JPL Manual*, Jet Propulsion Laboratory, Pasadena, California.

Kawamura, H. and P. Wu, 1998. Formation mechanism of Japan Sea Proper Water in the flux center off Vladivostok. *J. Geophys. Res.*, **103**: 21611-21622.

Kelly, K.A. and M.J. Caruso, 1999. A modified objective mapping technique for scatterometer wind data. *J. Geophys. Res.*, **95**: 13483-13496.

Kelly, K.A., S. Dickinson, and Z. Yu, 1999. NSCAT tropical wind stress maps: Implications for improving ocean modeling. *J. Geophys. Res.*, **104**: 11291-11310.

Kim C.H. and J.H. Yoon, 1996. Modeling of the wind-driven circulation in the Japan Sea using a reduced gravity model, *J. Oceanogra*, **52**: 359-373.

Lee, D.K., 1998. Ocean surface winds over the seas around Korea measured by the NSCAT (NASA Scatterometer). *J. Korean Soc. Remote Sensing*, **14**: 37-52.

Liu, W.T., K.B. Katsaros, and J.A. Businger, 1979. Bulk parameterization of air-sea exchanges of heat and water vapor including the molecular constraints at the interface. *J. Atmos. Sci.*, **36**: 1722-1735.

Na J.Y., J.W. Seo, and S.K. Han, 1992. Monthly-mean sea surface winds over the adjacent seas of the Korea Peninsular. *J. Korean Soc. Oceanogr.*, **27**: 1-10.

Na J.Y., S.K. Han, J.W. Seo, Y.G. Noh, and I.S. Kang, 1997, Empirical orthogonal function analysis of surface pressure, sea surface temperature and winds over the East Sea o the Korea (Japan Sea). *J. Korean Fish. Soc.*, **30**: 188-202.

Park, K.A. and P. Cornillon, 2002. Stability-induced modification of sea surface winds over Gulf Stream Rings. *Geophys. Res. Lett.*, **29**: 2211-2214.

Manuscript received October 1, 2003
Revision accepted December 26, 2003
Editorial handling: Yign Noh